Fine structure of the $1g_{9/2}$ isobaric analog resonance in ^{61}Cu

J. Sziklai and T. Vass
Central Research Institute for Physics, P.O. Box 49, Budapest 114, Hungary H-1525

J. A. Cameron
Tandem Accelerator Laboratory, McMaster University, Hamilton, Ontario, Canada L8S 4K1

I. M. Szöghy
Département de Physique, Université Laval, Québec, Québec, Canada G1K 7P4
(Received 19 July 1989)

Eleven fragments of the $1g_{9/2}$ isobaric analog state in ^{61}Cu have been found. To locate these fragments ^{60}Ni$(p,p_1\gamma)$ and ^{60}Ni$(p,\gamma)^{61}$Cu reactions were used. The excitation functions were measured in the $E_p^{lab}=3.67-3.83$ MeV proton energy range. To determine the spins of the resonances, γ angular distributions were measured. Partial widths for each resonance fragment were deduced and fine structure analyses were carried out in the different channels. The inelastic spectroscopic factor was derived for the $1g_{9/2}$ isobaric analog state. The results are compared with previous works.

I. INTRODUCTION

The $1g_{9/2}$ states in the f-p shell nuclei have been subjects of many studies. Because of their relative isolation and more or less simple shell-model structure, their identification is possible even in cases when the analog states are fragmented. The most important source of information on the fragmentation of the analog states is the R-matrix analysis of differential cross sections of (p,p_0) and (p,p_1) reactions.[1,2] Their sensitivity, however, is optimal mainly for the lower ($J \leq \frac{5}{2}$) spin resonances, due to penetrability reasons. For higher-spin resonances ($J \geq \frac{9}{2}$), proton capture seems to provide important details, where the principal γ decays proceed to other single-particle states, by isospin allowed $E1$ and $M1$-type isovector transitions, i.e., transitions to the antianalog $\frac{9}{2}^+$, or other $\frac{7}{2}^-$ states, and other higher-spin, i.e., $\frac{9}{2}^-$ and $\frac{11}{2}^-$ states are usually populated.

The $1g_{9/2}$ isobaric analog resonance (IAR) in ^{61}Cu corresponding to the $E_x=2.1216$-MeV parent state of strong single-particle character ($S_n=0.845$) in ^{61}Ni (Ref. 3) has been studied by several authors.[4-7] Szentpétery and Szücs[4] found this IAR fragmented and they identified three fragments based on the strong $M1$-type isovector γ decay of the fragments to the antianalog (AA) state. Adachi *et al.*[5] localized four fragments, using a high-resolution proton beam for elastic scattering differential cross section measurements on ^{60}Ni, together with their R-matrix analysis and the ^{60}Ni$(p,\gamma)^{61}$Cu reaction. Later Arai *et al.*[6] concluded that only three fragments were proved to be $1g_{9/2}$ fragments, and they found some energy difference with earlier results.[3] Bergdolt *et al.*[7] identified seven fragments based on the γ-decaying properties of the IAR. Their spin determination was based only on the γ branchings measured at different stronger peaks appearing in the integral excitation function, measured in the proton bombarding energy range of interest. For an ambiguous case, differential-type excitation functions were measured. No angular distribution measurements were made.

The behavior of the strength of the $M1$ analog to antianalog (A-AA) transition has been the subject of several studies.[8-11] Different core-excited states, e.g., core-polarized states (CPS)[9] and spin-flip states (SFS)[10] were introduced as being responsible for the hindrance of this transition. Shell-model calculations with four active shells[11] gave an improved agreement between the theory and the experimentally found relatively strong $\frac{9}{2}^+$-$\frac{9}{2}^+$ A-AA $M1$ transition. Considering the fragmentation of the single particle and analog states this can have an effect on the strengths of the A-AA transition too, since this transition can only be strong (i.e., close to the single-particle estimate), if neither analog nor antianalog states are fragmented. In the series of multi-channel studies[12-14] on the fragmentation of $1g_{9/2}$ isobaric analog resonances the ^{60}Ni$+p$ system was investigated, where in the daughter nucleus ^{61}Cu there are at least two $\frac{9}{2}^+$ states at low energies, thus showing, that the antianalog state in this case is fragmented.

II. EXPERIMENTAL PROCEDURE

The experiments were carried out at the FN Tandem Accelerator of the McMaster University. The typical proton beam resolution of $\sim$600 eV was achieved, and due to the computer controlled NMR stabilizer, it was kept even for longer exposures. The beam-energy calibration was obtained by reproducing the well-known $1g_{9/2}$ IAR in ^{59}Cu, at 3.547-MeV proton bombarding energy. Targets were prepared by electroplating (96.0)% ^{60}Ni onto thick (0.5-mm) high-purity gold backings. The target thickness was 11 μg/cm^2, corresponding to $\sim$700-eV energy loss for the 3.8-MeV protons.

The γ rays were detected by an n-type ORTEC Gamma

X high-purity germanium detector of 29% efficiency for the 1.333-MeV ^{60}Co line, and with energy resolution of ~8 keV for the 9-MeV γ rays. For excitation function measurements this detector was placed close to the target and oriented at 55° to the beam direction. For angular distribution measurements the same detector was placed at 10 cm from the target, carefully centered, and rotated in a series of 90°-0°-45°-60°-30° cycles. At −90° a second detector (26% ORTEC GammaX) was used as a monitor for the angular distribution measurements. The cycles of the moving detector were carried out by a stepper motor controlled by the VAX 11/750 computer through a set of an MBD-controlled CAMAC modules. Centering of the beam spot with respect to the detector circle was checked by measuring the angular distribution of the E_γ=0.842-MeV isotropic γ ray from the ^{27}Al$(p,p'\gamma)$ reaction and was found to be better than 1%.

The excitation functions were measured in the 3.670–3.830-MeV bombarding energy range in steps of ~640 eV. Typical target current was ~1.5 μA. The charge collected at each step was 1.2 mC. In cases when, due to the high level density and the finite-energy resolution, the resonances were not well resolved, differential excitation curves were also measured.

III. RESULTS

A. Excitation functions

The excitation functions measured in the E_p=3.670–3.830-MeV bombarding proton energy region in 640-eV steps are shown in Fig. 1. Forty-three resonances were found and analyzed in this region. Figure 1(a) shows the differential excitation function of the ^{60}Ni$(p,p_1\gamma)$ reaction. Besides some stronger peaks at the lower and higher end of the region, no intense peaks can be found in the central region of this IAR (around 3.730 MeV), showing that the inelastic strength of this $1g_{9/2}$ IAR, compared to other lower-spin resonances, cannot be too large.

Figures 1(b)–1(c) show integral excitation functions of the ^{60}Ni$(p,\gamma)^{61}$Cu reactions. The excitation function in Figs. 1(b) and 1(c) show mainly resonances populating the first and second fragment of the antianalog (AA1, E_x=2.721 MeV and AA2, E_x=4.132-MeV) states, respectively. All the fragments of the $1g_{9/2}$ IAR were expected to appear in these excitation curves. The excitation curve in Fig. 1(d) shows mainly resonances decaying to the ground state of ^{61}Cu, thus having spins $J_R \leq \frac{5}{2}$. Although, the structure of these excitation curves is rather complex, several intense peaks in the AA1 and AA2 windows show the presence of the analog state in the main γ-decay channels, but may be accompanied by a conflicting γ ray to levels of low spin.

B. Angular distributions and resonance spins

In order to find the fragments of the $1g_{9/2}$ IAR among the resonances present in the excitation curves, the spins of the resonances were determined by angular distribution measurements. For this purpose the decays to the first excited 2^+ state in ^{60}Ni and to the two fragments of the antianalog states (AA1 and AA2) were used.

For the analyses of the angular distributions in the $(p,p_1\gamma)$ channel the method of normalized angular distributions was used. The details of this procedure are given in Ref. 12. Figure 2 shows an example of how the $\frac{9}{2}$ spin was chosen for one of the fragments (resonance 16) of the IAR studied.

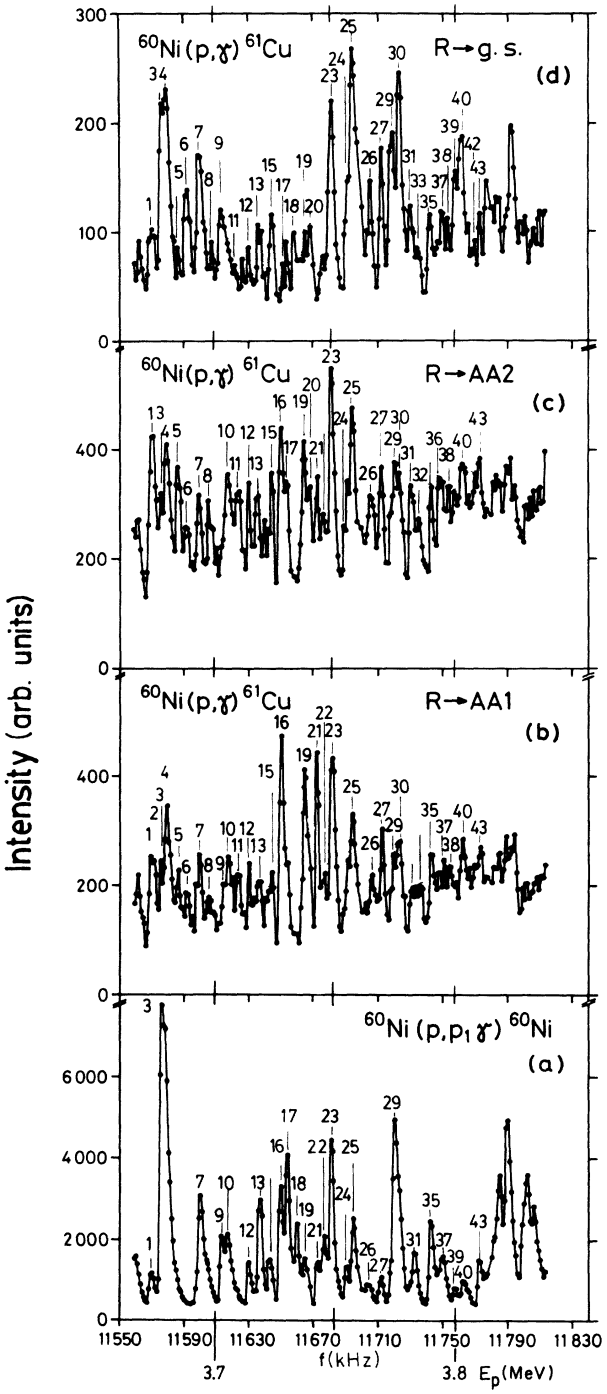

FIG. 1. Excitation functions for the ^{60}Ni$(p,p_1\gamma)^{60}$Ni and ^{60}Ni$(p,\gamma)^{61}$Cu reaction channels in the proton bombarding energy range of E_p=3.67–3.83 MeV measured in 640-eV steps.

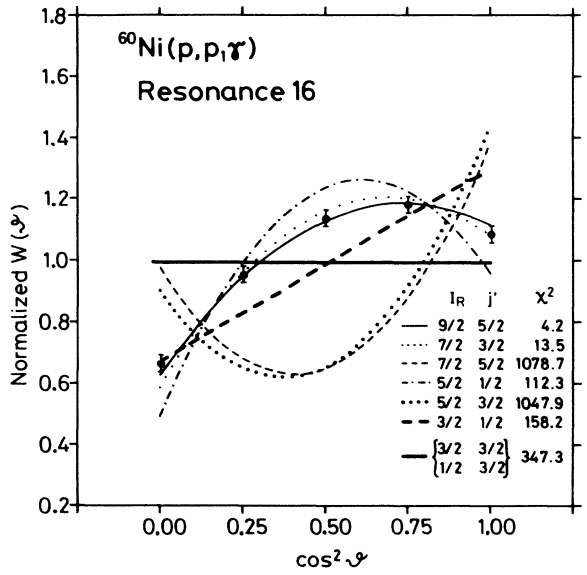

FIG. 2. Fits to the $(p,p_1\gamma)$ angular distribution measured at resonance 16. The data are best fitted assuming a resonance spin of $\frac{9}{2}$. The good spin selectivity for such isolated resonances provides independent information on the quality of data.

Since the angular distributions alone do not give unique and unambiguous spin and parity assignments for the resonances, some model-dependent considerations were also taken into account. Figure 3 shows the measured and fitted (p,γ) angular distributions of the γ transitions to the AA1 and AA2 states together with their χ^2 analyses. The isovector $M1$ γ transitions between the analog and antianalog states are isospin-allowed transitions, but the $E2$ transitions, which can mix with the $M1$ transitions, are isospin forbidden.[15] Thus, the $\frac{9}{2}$ spin was accepted only if this spin assumption gave the lowest χ^2 minimum with the lowest $\delta(E2/M1)$ mixing ratio. For resonance 16 (Fig. 3), the $\frac{9}{2}$-$\frac{9}{2}$ mixing ratio is indeed consistent with zero. Only those candidates were accepted as real $1g_{9/2}$ fragments where the results of the angular distribution analyses in the $(p,p_1\gamma)$ and in both (p,γ) channels agreed with the $1g_{9/2}$ resonance spin assumption simultaneously.

The angular distributions and their analyses for the other $1g_{9/2}$ IAR fragments in ^{61}Cu are shown in Figs. 4 and 5. Due to the limited energy resolution and the high-level density at this excitation energy in ^{61}Cu, the effects of neighboring low-spin resonances in the $(p,p_1\gamma)$ angular distributions on Figs. 4 and 5 are evident. The results of the decomposition by the method of normalized angular distribution[12] are given in percentages. The case of resonance 14 at $E_p=3721.0$ keV (Fig. 4) is very special, since the free, three-parameter fit (A_0,a_2,a_4) gave a value of $a_4=A_4/A_0=-0.738\pm0.015$. This very large negative a_4 value cannot originate from any single spin up to $J=\frac{13}{2}$. A possible solution might be to assume that two separate resonances with spins giving a relatively high a_4 value for this angular distribution, i.e., the $J=\frac{5}{2}(j'=\frac{1}{2})$ and $J=\frac{9}{2}(j'=\frac{9}{2})$ are experimentally mixed. To test this assumption the excitation function of the angular distribution of this $(p,p_1\gamma)$ reaction was measured. The result is given on Fig. 6. The analysis showed that the changes in the form of the angular distribution curves correspond to an increasing amount of $\frac{9}{2}$ strength: 17% at 11 640 kHz, 22% at 11 641 kHz, and 27% at 11 642 kHz. It is important to note that this $\frac{9}{2}$ decay is proceeding with $l'=4$ orbital momentum, which normally is not considered as a very possible way for such decays at this excitation energy to occur, due to reasons of penetrability. If it is present, however, it must have a fairly high reduced partial strength. It is evident that the inelastic width of this resonance will not contribute to the inelastic strength function of decay with "normal," $l'=2$ orbital momentum. Since the γ-decay properties and analyzed angular distribution measurements for the A-AA1 and A-AA2 decays for this resonance strongly support the $\frac{9}{2}$-spin assumption, this resonance was accepted as one of the $1g_{9/2}$ fragments which for some reason actually does not decay by "normal" $l'=2$ particle decay.

C. γ-branching ratios of the $\frac{9}{2}^+$ IAR fragments

Figure 7 shows the branching ratios for the primary γ decays from the fragments of the $1g_{9/2}$ IAR. To derive these deexcitation schemes the neighborhood of each resonance fragment was carefully examined, i.e., the measured differential excitation curves were analyzed. Only those primary transitions were included which showed clear resonance together with the most characteristic γ transition, i.e., A-AA1. Spins and parities of the levels fed by the primary transitions are taken from Ref. 3. The basic structure of these decay schemes is fairly simple. The main feature is a dominant $M1$ decay to the AA1 state. The importance of decays to other states changes from fragment to fragment. The population of levels with no assigned spins was observed only in spectra measured at the $1g_{9/2}$ resonance fragments. Their intensities, however, were not sufficient to allow us to determine their spins and parities. From their appearance in the resonant spectra one can assume their spins to be in the range of $\frac{7}{2}^-$, $\frac{9}{2}^-$, $\frac{9}{2}^+$, to $\frac{11}{2}^-$.

IV. FRAGMENTS OF THE $1g_{9/2}$ IAR

A. The $g_{9/2}$ resonances

Based on angular distribution measurements and γ-decay branching ratios, as described above, eleven $1g_{9/2}$ resonances were selected as fragments of the $1g_{9/2}$ IAR in ^{61}Cu. The relative errors of energies are considered to be ±0.5 keV. The absolute errors might be larger. Our energies agree quite well with those found by Bergdolt *et al.*,[7] while there exists a shift of about 7 keV compared to the Tokyo energies.

1. $E_p=3710.0$ keV, resonance 11

This resonance was identified by Bergdolt *et al.*[7] Their spin assignment, however, was not supported by angular

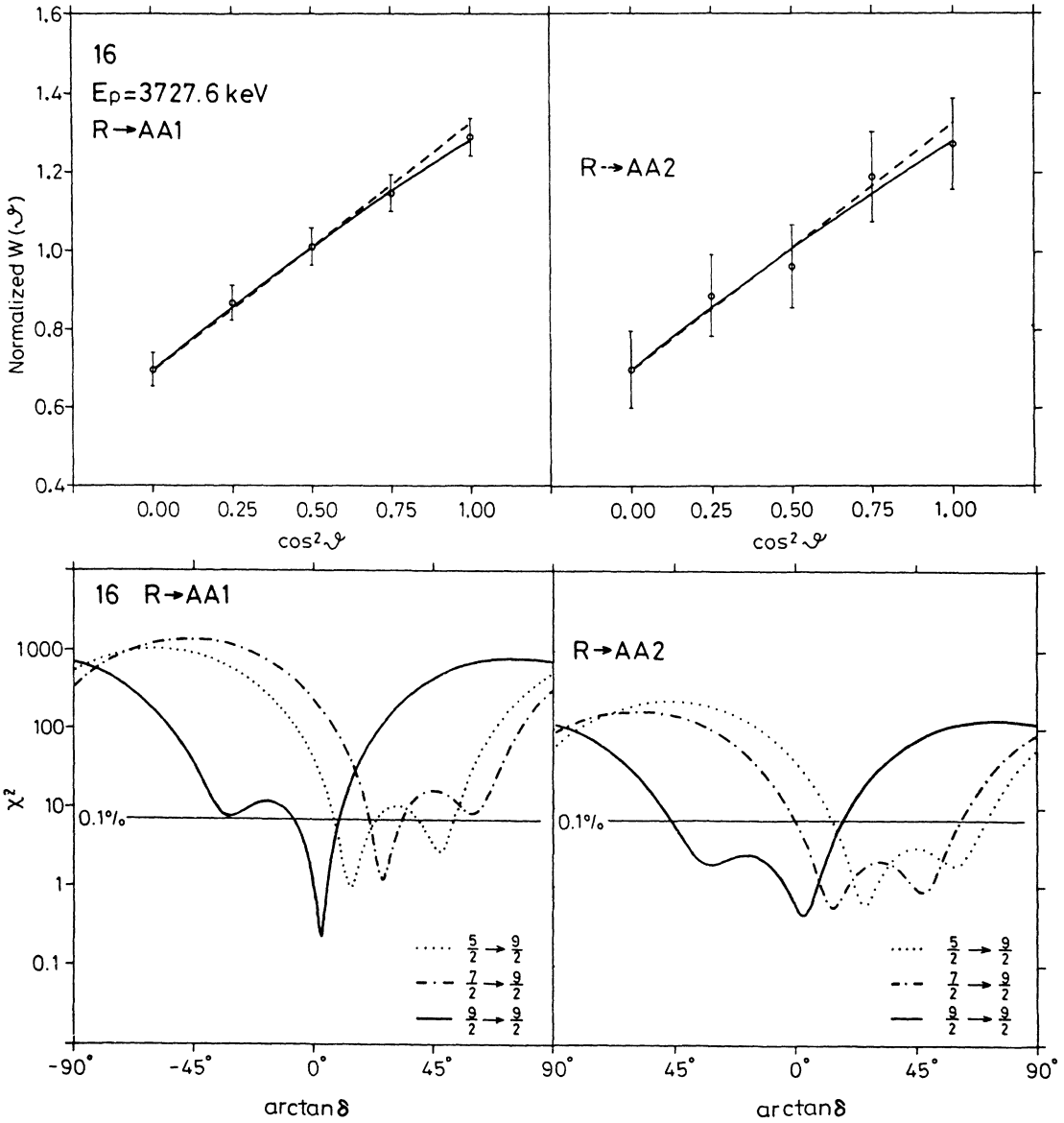

FIG. 3. Measured and fitted (p,γ) angular distributions for the A-AA1 and A-AA2 transitions together with their χ^2 analyses at resonance 16.

distribution measurements. The present angular distribution measurements on this resonance (see Fig. 4) strongly support the $\frac{9}{2}$-spin assignment. As can be seen from Fig. 7, this resonance decays only weakly to AA2; however, in spite of the relatively large experimental errors, the angular distribution of this transition also agrees with the $\frac{9}{2}$-spin assignment. The presence of a $\frac{3}{2}$-spin resonance in the angular distribution of the γ ray from ^{60}Ni$(p,p_1\gamma)$ reaction (47%) is clearly visible, though no such resonance was reported by Arai *et al.*[6]

2. $E_p = 3714.4$ keV, resonance 12

This resonance was also identified by Bergdolt *et al.*,[7] together with an unresolved $\frac{3}{2}$-spin resonance. The analysis of the angular distribution of the γ ray from the ^{60}Ni$(p,p_1\gamma)$ reaction (Fig. 4) shows the effect of a close-lying $\frac{3}{2}$-spin resonance (34%). This agrees well with the results of Bergdolt *et al.*[7]

3. $E_p = 3717.4$ keV, resonance 13

The angular distributions of γ rays going to AA1 and AA2 states strongly support the $\frac{9}{2}$-spin assignment. The γ branchings are also very similar to those of the other fragments, where the A-AA1 transition is the strongest one and several final states with spins $\frac{7}{2}$ to $\frac{11}{2}$ are also populated. This resonance fragment has not been reported earlier. The strong $\frac{3}{2}$ contribution in the $(p,p_1\gamma)$ an-

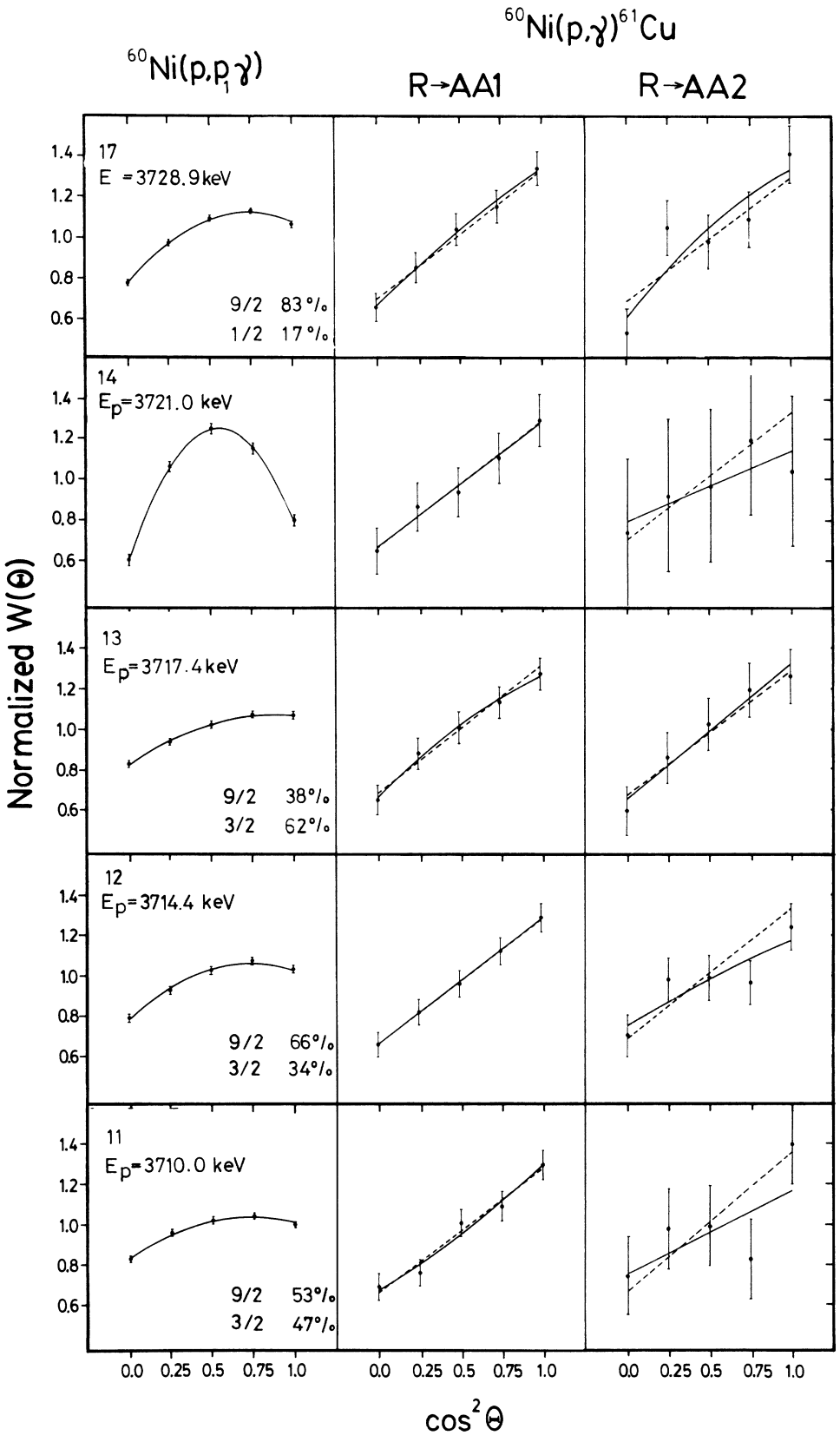

FIG. 4. Measured and fitted angular distributions of γ rays from ^{60}Ni$(p,p_1\gamma)^{60}$Ni and ^{60}Ni$(p,\gamma)^{61}$Cu reactions measured at resonances 11–14, and 17. The solid lines in the (p,γ) angular distributions are for the three-parameter free fits, while the dashed lines show the theoretical angular distributions for $\frac{9}{2}$-$\frac{9}{2}$ transitions.

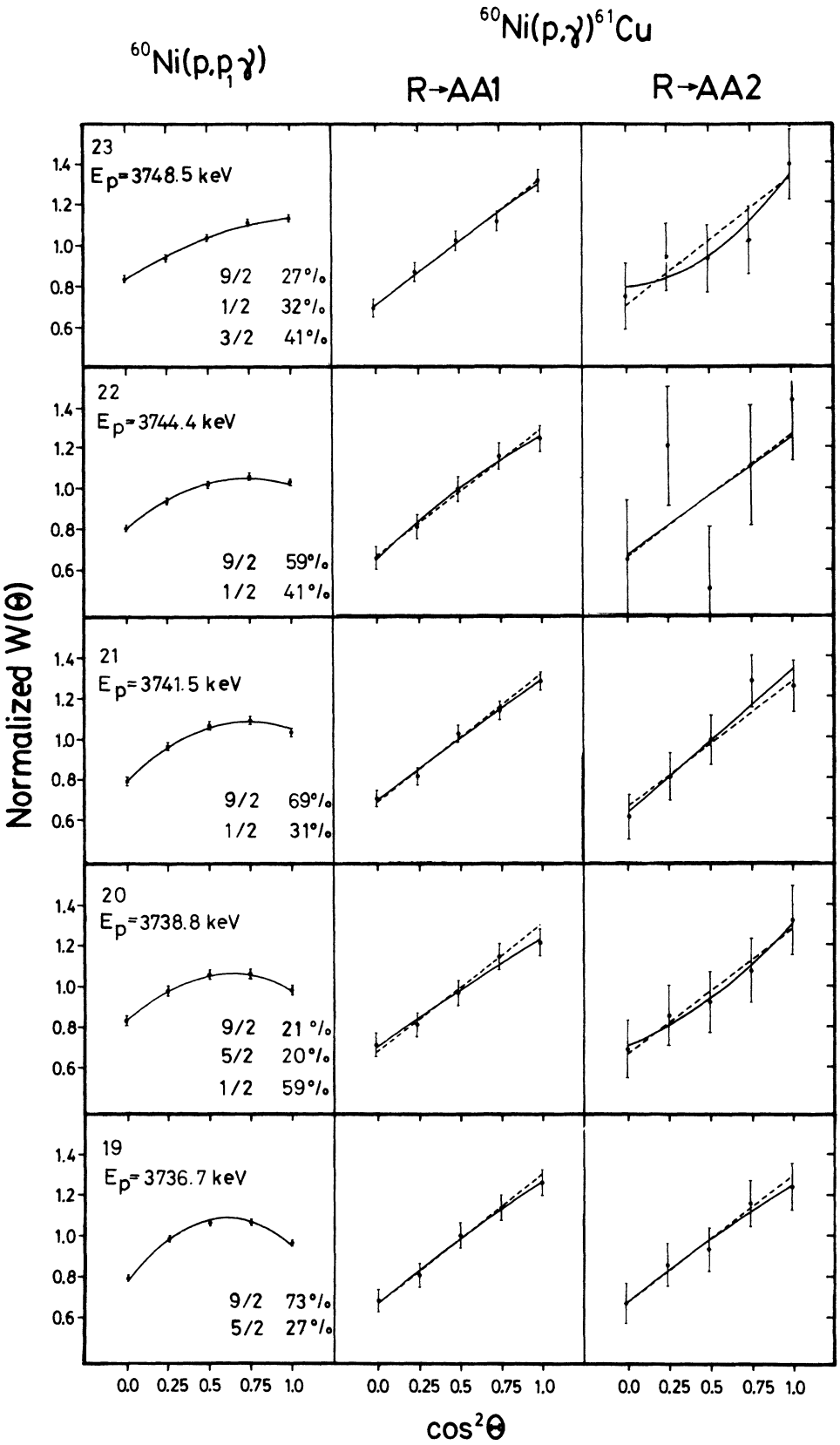

FIG. 5. Measured and fitted angular distributions of γ rays from ^{60}Ni$(p,p_1\gamma)^{60}$Ni and ^{60}Ni$(p,\gamma)^{61}$Cu reactions measured at resonances 19–22, and 23. The solid lines in the (p,γ) angular distributions are for the three-parameter free fits, while the dashed lines show the theoretical angular distributions for $\frac{9}{2}$-$\frac{9}{2}$ transitions.

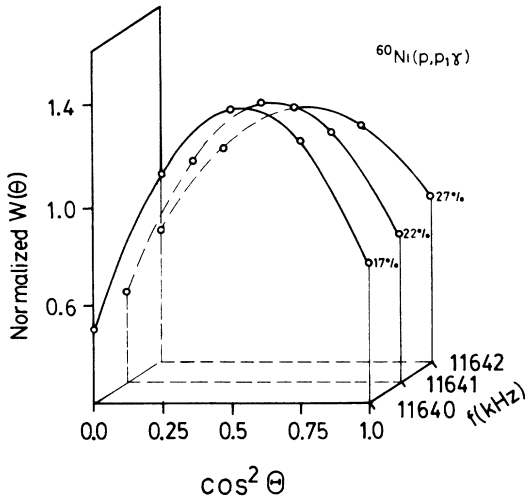

FIG. 6. Excitation function of the $(p,p_1\gamma)$ angular distribution in the vicinity of resonance 14.

gular distribution may originate from the $\frac{3}{2}^-$ resonance, reported at $E_p = 3709$ keV by Arai *et al.*[6]

4. $E_p = 3721.0$ keV, resonance 14

This resonance was also found by Bergdolt *et al.*[7] The decay scheme of this fragment is similar to that of resonance 13. The angular distributions of the primary γ rays to AA1 and AA2 states, in spite of the relatively large errors, are consistent with the $\frac{9}{2}$-spin assignment. The case of the $(p,p_1\gamma)$ angular distribution was discussed in detail in the previous section.

5. $E_p = 3727.6$ keV, resonance 16

Considering its yield, this is one of the strongest fragments, and was seen in all previous studies.[1–7] Angular distributions and their analyses clearly show the validity of spin assignments of $\frac{9}{2}$ (Figs. 2 and 3). The γ-decay properties of this resonance are fairly simple, i.e., in 64%

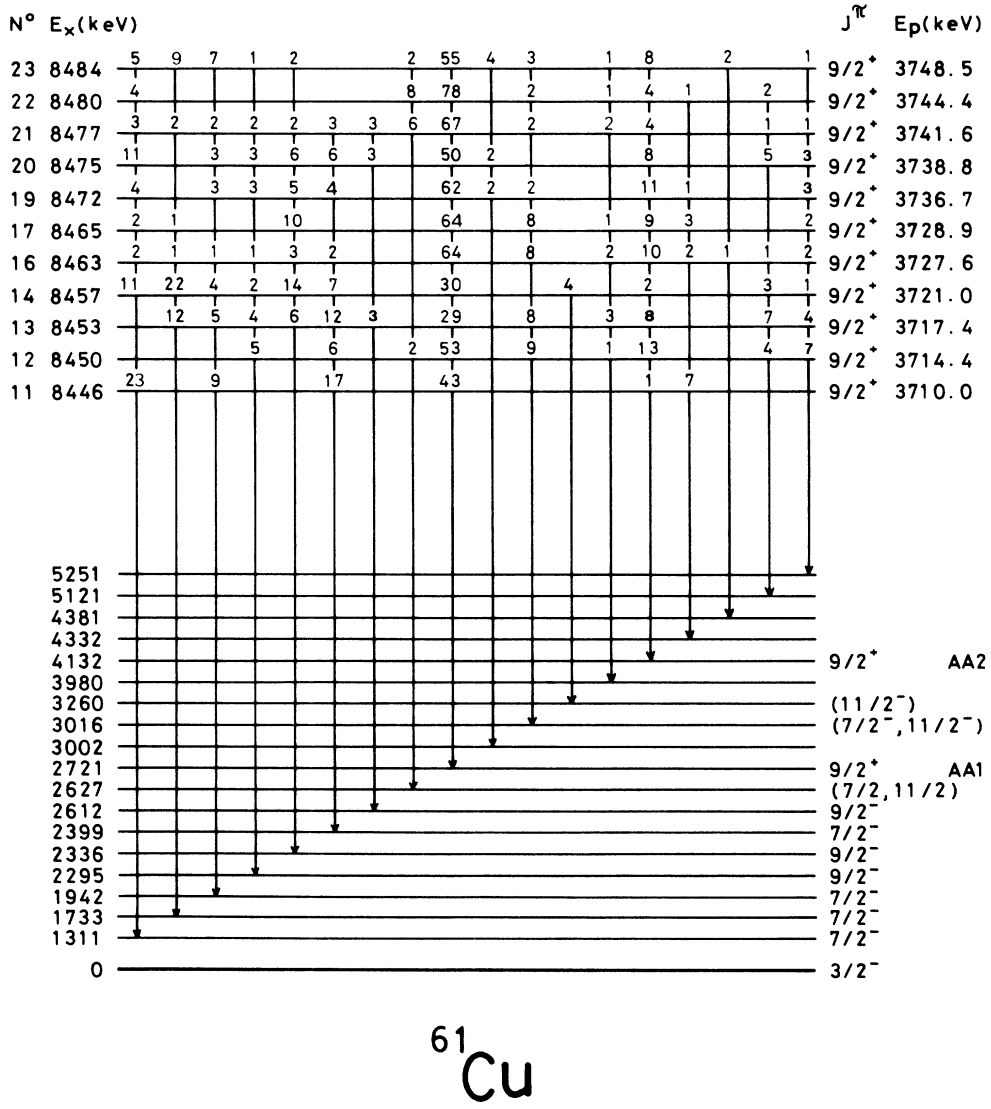

FIG. 7. γ branchings for the identified $1g_{9/2}$ IAR fragments in ^{61}Cu.

it decays to AA1, in 10% to AA2, and the remaining strength goes to different $J=\frac{7}{2}$-spin states.

6. $E_p=3728.9$ keV, resonance 17

Bergdolt *et al.*[7] reported a resonance at $E_p=3730.1$ keV with spin $\frac{1}{2}$ or $\frac{3}{2}$. Measured angular distributions (Fig. 4) strongly support the spin assignment $\frac{9}{2}$ for this resonance. The 17% $J=\frac{1}{2}$-spin inelastic contribution, found in the $(p,p_1\gamma)$ angular distribution agrees with the suggestion of the Bergdolt *et al.*[7] The strength of this resonance is weaker than that of resonance 16, but the γ-decay properties are very similar.

7. $E_p=3736.77$ keV, resonance 19

This resonance was also seen in all previous works on this IAR. The present angular distribution measurements and their analyses (Fig. 5) strongly support the $\frac{9}{2}$-spin assignment. The γ-decaying propeties are fairly similar to that of resonance 16.

8. $E_p=3738.8$ keV, resonance 20

Bergdolt *et al.*[7] reported a resonance at $E_p=3739.3$ keV with spin $\frac{1}{2}$ or $\frac{3}{2}$. Measured angular distributions (Fig. 5) support the spin assignment $\frac{9}{2}$ for this resonance. The γ branchings also support the $\frac{9}{2}$-spin assignment, since the most important γ decay is the isovector A-AA1 transition.

9. $E_p=3741.6$ keV, resonance 21

This resonance is also one of the strongest fragments, and was seen in all previous studies.[4–7] It appears in all excitation functions and the angular distributions and their analyses agree with the spin assignment of $\frac{9}{2}$ (Fig. 5). The $(p,p_1\gamma)$ angular distribution shows the presence of a close-lying spin-$\frac{1}{2}$ resonance. The observed γ branching also supports the $\frac{9}{2}$-spin assignment.

10. $E_p=3744.4$ keV, resonance 22

This resonance is one of the new fragments. The angular distributions and their analyses (Fig. 5) all support the spin assignment of $\frac{9}{2}$. The $(p,p_1\gamma)$ angular distribution shows the effect of an unresolved spin-$\frac{1}{2}$ resonance. This might originate from a nearby, wide $p_{1/2}$ resonance ($\Gamma_p=1222$ eV) reported by Arai *et al.*[6] at $E_p=3739$-keV bombarding energy. The γ-decay properties of this resonance are the simplest. Its 78% decay to AA1 supports the assumption $\frac{9}{2}$ for this resonance too.

11. $E_p=3748.5$ keV, resonance 23

There is a very strong g.s. ($\frac{3}{2}^-$) transition in the spectra measured at this resonance. This transition, therefore, cannot be considered as one originating from a $\frac{9}{2}$-spin resonance. The angular distributions of γ rays to AA1 and AA2 states, and their analyses strongly support the spin assignment of $\frac{9}{2}$ for this resonance. The angular distribution in the $(p,p_1\gamma)$ channel shows the presence of unresolved $\frac{1}{2}$ and $\frac{3}{2}$ spin resonance in our spectra, thus explaining the very strong R-g.s. transition.

B. The absolute yields of the resonance fragments

From the analysis of the γ-ray spectra the absolute yields were calculated, using Gove's formulae[16]

$$\omega_\gamma=\frac{2\epsilon}{\lambda^2}Y(\infty,\infty)=\frac{2J+1}{2}\times\frac{\Gamma_p\Gamma_\gamma}{\Gamma}\ , \tag{1}$$

$$\omega_{p_1}=\frac{2\epsilon}{\lambda^2}Y(\infty,\infty)=\frac{2J+1}{2}\times\frac{\Gamma_p\Gamma_{p_1}}{\Gamma}\ , \tag{2}$$

where ϵ is the stopping power of the target material in keV cm^2/atom, λ is the wavelength of protons of energy E_p in cm, $Y(\infty,\infty)$ is the thick target yield, J is the spin, Γ_p is the proton partial width, Γ_γ is the gamma partial width, Γ_{p_1} is the proton inelastic width, and Γ is the total

TABLE I. Yields calculated from our data and their comparison with results from Ref. 7.

	a				b	
N^0	E_p (keV)	ω_{AA1}	ω_{AA2} (eV)	ω_{pp_1}	E_p (keV)	ω_{AA1} (eV)
11	3710.0	0.19	0.01	2.79	3709.1	0.16
12	3714.4	0.35	0.09	9.13	3714.3	0.74
13	3717.4	0.19	0.06	3.32		
14	3721.0	0.20	0.02	2.86	3721.6	0.26
16	3727.6	1.41	0.22	29.12	3727.7	1.32
17	3728.9	0.90	0.12	24.33		
19	3736.7	1.12	0.20	0.79	3736.7	1.21
20	3738.8	0.50	0.08	0.61		
21	3741.6	1.33	0.09	11.31	3741.7	1.17
22	3744.4	0.25	0.01	7.03		
23	3748.5	0.59	0.08	2.24	3747.1	0.57

[a]Present work.
[b]Reference 7.

TABLE II. Deduced proton partial widths and their comparison with results given in Refs. 5 and 6.

N^0	E_p (keV)	Γ_p (eV) a	b	c
11	3710.0	2.0		
12	3714.4	3.9		
13	3717.4	2.0		
14	3721.0	2.1		
16	3727.6	14.9	14.8	11.2
17	3728.9	9.5		
19	3736.7	11.9	6.3	7.1
20	3738.8	5.2		
21	3741.6	14.0	8.3	6.7
22	3744.4	2.5		
23	3748.5	6.1		

[a]Present work.
[b]Reference 5.
[c]Reference 6.

width of the resonance.

The absolute yields obtained in the present work are summarized in Table I and compared with those of Bergdolt *et al.*[7] To derive errors for the yields, the rules of error propagation were used resulting in errors $\approx 10\%$ for the strongest, and $\approx 25\%$ for the weaker fragments. It can be seen from Table I that our results are in good agreement with those of Bergdolt *et al.*[7] for resonances and channels seen in both works. The only disagreement is resonance 12, where Bergdolt *et al.*[7] found more than twice the yield we obtained. The possible cause for the difference might arise from the way the yields were derived. Bergdolt *et al.*[7] used Γ_p/Γ_{p_1} ratios given by Adachi *et al.*[5] or the $\Gamma_p \approx \Gamma_{p_1}$ assumption, while we used a more detailed assumption, because, unfortunately no Γ_p values were available for most of the fragments. The spectroscopic factor of the parent state was used to derive these elastic partial widths by taking

$$S_n = S_{pp} = (2T_0+1) \sum \Gamma_p / \Gamma_{\text{s.p.}} , \tag{3}$$

where S_n is the neutron spectroscopic factor of the parent state, S_{pp} is the proton spectroscopic factor of the analog state, T_0 is the isospin of the target nucleus, $\sum \Gamma_p$ stands for the sum of the elastic partial widths for the IAR, and $\Gamma_{\text{s.p.}}$ is the single-particle width calculated with the program HANS.[17] The sum of the partial widths was calculated from Eq. (3). This total strength was then distributed among the fragments in proportion with the yields of ω_{AA1}. The idea behind this procedure is that the parent $1g_{9/2}$ state,[3] as well as the IAR, is of single-particle character. Thus, it decays with high probability to states with similar structure, e.g., to AA1. The yield of this decay is supposed to be proportional to the core+$1p$ part of the wave function of the IAR, thus being proportional to the strength of the elastic proton decay. The Γ_p values derived with this procedure are given in Table II, together with experimental values from Refs. 5 and 6. It can be seen that our values are in good agreement with the experimental ones. Our derived Γ_p for resonance 21, however, is much larger than the experimental one.

C. The deduced partial widths of the $1g_{9/2}$ fragments

With the estimated Γ_p values now available for all of the fragments, the partial widths for all populated channels were calculated. The total width was considered to be the sum of all partial widths, i.e.,

$$\Gamma = \Gamma_p + \Gamma_{p_1} + \Gamma_{\text{AA1}} + \Gamma_{\text{AA2}} + \sum \Gamma_x , \tag{4}$$

where the sum in the last term stands for γ transitions other than the A-AA1 and A-AA2 transitions. The derived partial widths are given in Table III, and compared with the A-AA1 partial widths given by Bergdolt *et al.*[7] As it can be seen from Table III, there is a general agreement between our results and those of Bergdolt *et al.*[7] Any differences may be due to the differences in the ways the ratio of Γ_p/Γ_{p1} was derived in the two works.

TABLE III. Deduced partial widths and their comparison with results from Ref. 7. Asterisk: $l'=4$.

	Present work					Bergdolt *et al.*[7]	
N^0	E_p (keV)	Γ_{AA1} (meV)	Γ_{AA2} (meV)	Γ_{pp_1} (eV)	$\gamma^2_{p_1}$ (keV)	E_p (keV)	Γ_{AA1} (meV)
11	3710.0	56	2	0.8	0.13	3709.1	46
12	3714.4	142	34	3.7	0.59	3714.3	151
13	3717.4	62	18	1.1	0.17		
14	3721.0	61	5	0.9	9.60*	3721.6	72
16	3727.6	486	75	10.1	1.54	3727.7	494
17	3728.9	393	52	10.6	1.62		
19	3736.7	284	50	2.7	0.41	3736.7	281
20	3738.8	107	16	0.1	0.02		
21	3741.6	328	21	2.8	0.41	3741.7	228
22	3744.4	119	7	3.4	0.50		
23	3748.5	208	29	4.3	0.62	3747.1	311

TABLE IV. Spectroscopic factors for the $1g_{9/2}$ IAR in ^{61}Cu. For details on differences in the values of the spectroscopic factors derived by different methods see references given in text.

E_x^{parent} (MeV)	S_n	S_{pp_1} (TAR)	(ZDH)	(MM)
2.1216	0.845	0.219	0.176	0.175

TABLE VI. Comparison of the Coulomb displacement energies for the $1g_{9/2}$ IAR in ^{61}Cu.

ΔE_C (keV)				
Present work	Budapest '72 Ref. 4	Tokyo '74 Ref. 5	Tokyo '76 Ref. 6	Strasburg '76 Ref. 7
9369(1)	9354(14)	9381(9)	9372(10)	9381

D. Inelastic spectroscopic factor

From the sum of the inelastic partial widths, the inelastic spectroscopic factor was derived using the same formula as given in Eq. (3), with the exception that the single-particle width was calculated with energy and angular moments the same as those of the inelastically scattered protons. The resulting inelastic spectroscopic factors are given in Table IV. The derived values are large, however, the value by the Thomson-Adams-Robson (TAR) method is larger than the ones calculated with the Zaidi-Darmodjo-Harvey (ZDH) or the Mekjian-MacDonald (MM) method. The difference is $\approx 24\%$. Thus follows the systematics cited in papers listed under Ref. 25 in Ref. 12. The large inelastic spectroscopic factor reflects the importance of the 2^+ core excitation in the wave functions of the analog and parent states.

V. FINE STRUCTURE ANALYSES

After deriving and calculating the partial widths in different channels, fine structure analyses were performed independently in all channels. To remove the effect of the Coulomb barrier the γ_λ^2 reduced partial widths were used for the fine structure analysis in the (p,p_1) channel, but for the γ channels the Γ_γ partial widths were suitable. For the fine structure analyses the method of MacDonald-Mekjian-Kerman-De Toledo Piza[18,19] (MMKP) was used. The Lorentz-weighted average of the experimental partial widths, i.e., the experimental strength function

$$S(E;I)=\langle \gamma_\lambda^2/D_\lambda \rangle = \frac{1}{\pi}\sum_\lambda \frac{\gamma_\lambda^2}{(E-E_\lambda)^2+I^2} \ . \tag{5}$$

where D_λ is the mean level spacing, and I is the width of the Lorentz weight of averaging, was least-squares fitted to the parametric form of the doorway strength function[20]

$$S^D(E;I)=S_0+\frac{1}{\pi}\frac{\gamma^2_{\text{Analog}}}{\cos^2\phi} \times \frac{(I+\Gamma_S/2)\cos 2\phi-(E-E_{\text{Analog}})\sin 2\phi}{(E-E_{\text{Analog}})^2+(I+\Gamma_S/2)^2} \ , \tag{6}$$

where S_0 stands for the background strength function, γ^2_{Analog} is the total reduced width of the analog state, Γ_S is the spreading width, and E_{Analog} is the analog-state energy. The parameter ϕ describes the asymmetry of the strengths around the position of the analog state. The results of the analyses are listed in Table V. The experimental and fitted strength functions for the (p,p_1) inelastic channel, and for eight (p,γ) channels are given in Figs. 8 and 9.

VI. DISCUSSIONS

Table V lists the fine structure parameters in all decay channels. In spite of the fact that the analyses were carried out independently in different channels, there is a generally good agreement among the results obtained ex-

TABLE V. Fine structure parameters for the $1g_{9/2}$ IAR's in ^{61}Cu for the ^{60}Ni$(p,p_1\gamma)$ and all different ^{60}Ni$(p,\gamma)^{61}$Cu reaction channels. Asterisk: deduced.

Reaction	E_{Analog} (keV)	S_0 (eV)	Γ_{Analog} (eV)	Γ_s (keV)	tanΦ	I (keV)
$(p,p_0)^*$	3732.3(2)	−1.6(2)	18.17(2)[a]	7(1)	0.002(1)	14
$(p,p_1\gamma)$	3730.7(1)	−0.7(1)	6.14(1)[b]	7(1)	0.000(1)	14
(P,γ_{AA1})	3732.8(1)	−0.2(1)	2.23(1)	7(1)	0.001(1)	14
(p,γ_{AA2})	3730.9(1)	−0.04(1)	0.32(1)	7(1)	0.000(1)	14
$(p,\gamma_{1310.5})$	3732.1(3)	−0.03(1)	0.17(1)	12(2)	0.004(2)	20
$(p,\gamma_{1732.6})$	3731.7(3)	−0.03(1)	0.13(1)	13(2)	0.003(2)	20
$(p,\gamma_{1942.5})$	3733.2(4)	−0.03(1)	0.10(1)	14(2)	0.004(3)	20
$(p,\gamma_{2295\ 1})$	3730.4(3)	−0.01(1)	0.07(1)	10(2)	0.001(3)	20
$(p,\gamma_{2336\ 5})$	3730.5(1)	−0.02(1)	0.18(1)	4(1)	0.000(1)	14
$(p,\gamma_{2399\ 0})$	3725.3(1)	−0.03(1)	0.14(1)	10(2)	0.001(2)	20

[a] γ_0^2 (keV).
[b] $\gamma_{p_1}^2$ (keV).

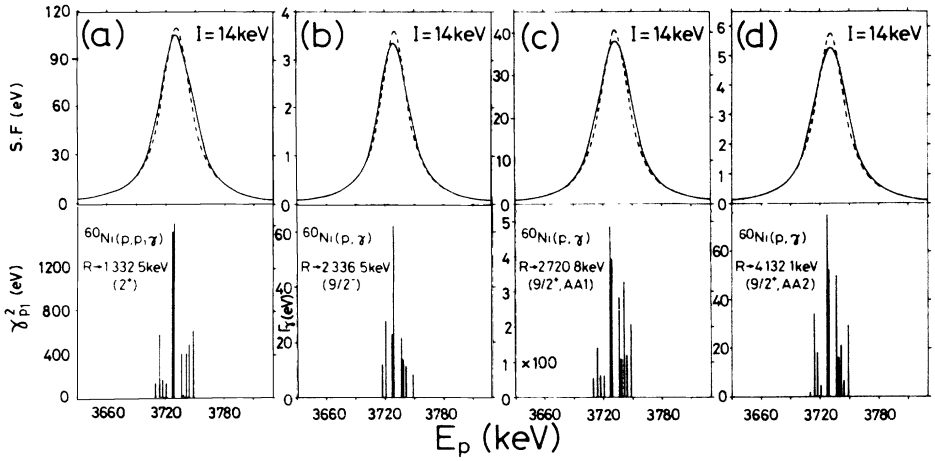

FIG. 8. Distribution of the partial widths and the fitted strength functions for the $1g_{9/2}$ IAR in ^{61}Cu for decay channels belonging to the first group (see text). The full curves are the five-parameter theoretical strength functions of the MMKP type. The broken lines are the Lorentz-averaged (half-width I) experimental strength function.

cept for the values for the spreading widths. The position of the analog state is closely the same in all channels, except for the γ channel to the $E_x = 2399.0$ keV ($\frac{7}{2}^-$) state which was not populated from the high-lying fragments (Fig. 7). Thus, the analog-state energy is about 5 keV lower in this γ-channel than in all other channels. The background strength functions are all small negative numbers reflecting the fact that there would be only very weak $T_< \frac{9}{2}$ strengths for the hallway states if the analog state were absent. The asymmetry parameter ϕ is practically zero for all the channels showing that there is no asymmetry found for this IAR. The only discrepancy that appeared among the fine-structure parameters found in different channels, is the difference in the spreading widths. The errors for the fine-structure parameters given in Table V are relatively small considering the uncertainty of the partial widths as input parameters for the fine-structure analyses. In a previous study on the error propagation in fine-structure analysis detailed in the appendix of Ref. 12, however, it was shown that the various parameters have quite different sensitivity for errors of the input data. Since the spreading width showed only a moderate sensitivity for the uncertainties in the input data, it seems reasonable to draw certain conclusions. Based on the spreading widths given in Table V, one can divide the decay channels into two categories: (1) Channels where the spreading width is ~ 7 keV, and $I = 14$ keV was the averaging interval where the parameters became independent of I. (2) Channels where the spreading width is ≥ 10 keV, and an $I = 20$ keV averaging interval was needed to make the parameters independent of I.

The first category includes the elastic, the inelastic, and the two AA channels, while all the other γ channels belong to the second category. It seems that there is a non-negligible difference in the spreading widths in different channels, as it was also found in some earlier stud-

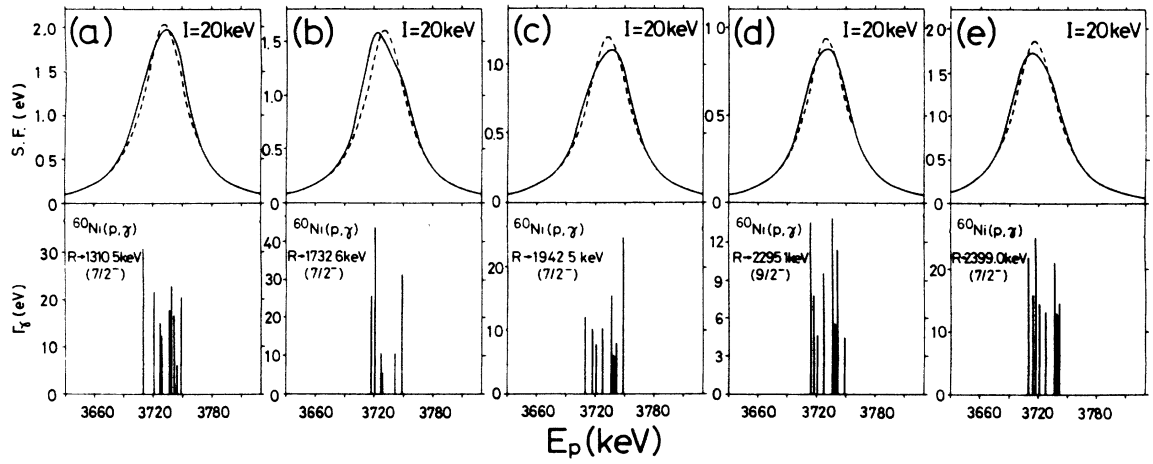

FIG. 9. Distribution of the partial widths and the fitted strength functions for the $1g_{9/2}$ IAR in ^{61}Cu for decay channels belonging to the second group (see text). The full curves are the five-parameter theoretical strength functions of the MMKP type. The broken lines are the Lorentz-averaged (half-width I) experimental strength function.

TABLE VII. Absolute analog-antianalog isovector $M1$ transition strengths of the $1g_{9/2}$ IAR fragments in ^{61}Cu nucleus, in Weisskopf units (in W.u.$\times 10^{-3}$).

		$B(M1)$			
	E_p	Present work		Ref. 6	Ref. 7
N^0	(keV)	IAS-AA1	IAS-AA2	IAS-AA1	IAS-AA1
11	3710.0	14.3	1.0		6.8
12	3714.4	36.3	20.5		18.2
13	3717.4	15.8	10.9		
14	3721.0	11.1	4.6		8.8
16	3727.6	123.9	44.7	160.0	83.3
17	3728.9	100.0	31.0		
19	3736.7	72.0	29.6	100.0	50.5
20	3738.8	27.1	9.5		
21	3741.6	82.9	12.5	80.0	45.4
22	3744.4	30.1	3.9		
23	3748.5	52.3	17.2	20.0	31.6
$\sum B(M1)$ (W.u.)		0.57	0.19	0.36	0.24

Present total $\sum B(M1)=0.76$ W.u.

ies.[1,12,14,21] If this difference is larger than the expected fluctuation of Γ_s for a relatively small sample size (as it is true for the present case since only 11 fragments were found), it can not be understood within the framework of the available theories[18–20] where the spreading width of the analog state is the property of the analog state itself, and not the channels where the analog state decays to. Unfortunately the limits of the fluctuations of Γ_s for the present case are not available; thus, it is hard to draw too serious conclusions regarding the occurred channel dependence of the spreading width. However, the spreading widths for the channels of the second category were found almost twice as large as in the first category.

Considering the members of the first category, the centroid of the fragmented $1g_{9/2}$ analog state was calculated to be $E^{\rm lab}_{\rm Analog}=3731.1\pm0.8$ keV. This corresponds to $E^{\rm cm}_{\rm Analog}=3670.4\pm0.8$ keV. The Coulomb displacement energy ΔE_C was calculated using the neutron separation energy of $B_n=7820.0$ keV for the parent ^{61}Ni nucleus[22] and the $E_X=2121.6$-keV excitation energy of the parent state.[3] Table VI gives the Coulomb displacement energy for the $1g_{9/2}$ analog state and its comparison with previous results. The present value is higher than the one given in Ref. 4, but smaller than the values of Refs. 5 and 7. The difference may originate from the fact, that, to calculate the centroid of the analog state, different numbers of fragments and different methods for centroid calculations were used in various laboratories.

From our data, absolute A-AA transition strengths were calculated. The results for the two fragments of the AA state are compared with previous results in Table VII. It can be seen that summing up the $B(M1)$ strengths going to AA2 gives $\sim$25% of the total $M1$ strength, showing that the structure of this AA2 state must be of simple character. Otherwise this transition would not be so important. The total $M1$ strength for the analog state is 0.76 W.u., which amounts to about 41% of the single-particle estimate. Thus, a considerable part of the total $M1$ single-particle strength was found in the present experiment. To understand this decrease of the strength which is not very severe, we can consider the fragmentation of the initial and final states with simple structure in the following ways: (1) If the AA state is not fragmented, but the parent state is, i.e., only a portion of the single-particle strength is found in the parent state, hindrance of the A-AA transition can be expected even in cases where the analog state is not fragmented. (2) If the analog state is fragmented due to the doorway-hallway coupling, but there is only one AA state, the $M1$ strength is also hindered. (3) Where both the analog and antianalog states are fragmented, the relative weakness of this $M1$ transition is almost "natural," since the basic condition for the strong A-AA transition, i.e., the simple and similar structure of the initial and final states, is obviously not satisfied, due to the fragmentation. The latter case may apply to the present analog state. However, in spite of the fragmentation a considerable amount (41%) of the single-particle A-AA $M1$ strength was found.

ACKNOWLEDGMENTS

The authors wish to express their gratitude to the staff of the McMaster Tandem Accelerator Laboratory for the excellent condition of the machine, and are indebted to the Natural Sciences and Engineering Research Council of Canada and the National Scientific Research Foundation of the Hungarian Academy of Sciences (Contract No. 1779) for financial support.

[1]E. G. Bilpuch, A. M. Lane, G. E. Mitchell, and J. D. Moses, Phys. Rep. **28C**, 145 (1976).
[2]G. E. Mitchell, E. G. Bilpuch, J. R. Shriner, and A. M. Lane, Phys. Rep. **117**, 1 (1985).
[3]L. P. Ekström and J. Lyttkens, Nucl. Data Sheets **38**, 496 (1983).
[4]I. Szentpétery and J. Szücs, Phys. Rev. Lett. **28**, 378 (1972).
[5]M. Adachi, T. Hattori, E. Arai, M. Ogawa, and H. Satoh, J. Phys. Soc. Jpn. **36**, 1266 (1974).
[6]E. Arai, M. Ogawa, and H. Satoh, Nucl. Phys. **A256**, 127 (1976).
[7]G. Bergdolt, A. M. Bergdolt, H. V. Klapdor, and M. Schrader, Nucl. Phys. **A263**, 477 (1976).
[8]S. Maripuu, Nucl. Phys. **A123**, 357 (1969).
[9]S. Maripuu, Phys. Lett. **31B**, 181 (1970).
[10]M. Hirata, Phys. Lett. **32B**, 656 (1970).
[11]S. Maripuu, J. C. Manthuruthil, and C. Poitier, Phys. Lett. **41B**, 148 (1972).
[12]J. Sziklai, J. A. Cameron, and I. M. Szöghy, Phys. Rev. C **30**, 490 (1984).
[13]J. Sziklai, J. A. Cameron, and I. M. Szöghy, in *Capture Gamma-Ray Spectroscsopy and Related Topics,* Proceedings of the Fifth International Symposium on Capture Gamma-Ray Spectroscopy and Related Topics, AIP Conf. Proc. No. 125, edited by S. Raman (AIP, New York, 1984).
[14]G. U. Din and J. A. Cameron, Phys. Rev. C **35**, 448 (1987).
[15]H. E. Gove, in *Nuclear Reactions,* edited by P. M. Endt and M. Demeur (North-Holland, Amsterdam, 1959), p. 259.
[16]E. K. Warburton and J. Weneser, in *Nuclear Physics,* edited by D. H. Wilkinson (North Holland, Amsterdam, 1969).
[17]H. L. Harney (unpublished). See details in Ref. 12.
[18]W. M. MacDonald and A. Z. Mekjian, Phys. Rev. **160**, 730 (1967).
[19]A. K. Kerman and A. F. R. De Toledo Piza, Ann. Phys. (N.Y.) **48**, 183 (1968).
[20]W. M. MacDonald, Ann. Phys. (N.Y.) **125**, 253 (1980).
[21]W. A. Watson III, E. G. Bilpuch, and G. E. Mitchell, Phys. Rev. C **24**, 1992 (1981).
[22]A. H. Wapstra and K. Bos, At. Data Nucl. Data Tables **19**, 215 (1977).